IEEE Access
Multidisciplinary ⋮ Rapid Review ⋮ Open Access Journal

Received 2 December 2023, accepted 2 January 2024, date of publication 8 January 2024,
date of current version 12 January 2024.

Digital Object Identifier 10.1109/ACCESS.2024.3350644

RESEARCH ARTICLE

Series Arc Fault Identification Method Based on Lightweight Convolutional Neural Network

AIXIA TANG[1], ZHIYONG WANG[1], (Member, IEEE), SHIGANG TIAN[1], (Student Member, IEEE), HONGXIN GAO[1], (Member, IEEE), YONG GAO[1], AND FENGYI GUO[2], (Senior Member, IEEE)

[1]Faculty of Electrical and Control Engineering, Liaoning Technical University, Huludao 125105, China
[2]College of Electrical and Electronic Engineering, Wenzhou University, Wenzhou 325035, China

Corresponding author: Fengyi Guo (20195207@wzu.edu.cn)

This work was supported by the National Natural Science Foundation of China under Grant 52077158.

ABSTRACT The fast and accurate series arc fault (SAF) identification method and its hardware implementation are the key to the development of arc fault circuit interrupter (AFCI) or arc fault detection device (AFDD). The SAF experiments under household multi-branch circuit conditions were conducted. And a novel SAF identification model based on lightweight one-dimensional (1-D) convolutional neural network was proposed. First, the main-circuit current signal was used as the input of the model. The 1-D convolutional layers and 1-D maximum pooling layers of the model were used to extract the features of the current signal. The fully connected neural network (FCNN) was used to identify whether or not there is a SAF in the circuit and determine the branch-circuit where the fault is located. Second, the second to fourth standard convolutional layers of the model were improved by using depthwise separable convolution, and the batch normalization layers were added to the model, so as to realize the optimal design of the model. Finally, the model was deployed to an embedded device and its performance was tested. When the sampling frequency is higher than 5 kHz, the accuracy of fault identification and fault line selection of the model in the embedded device is higher than 98.05% and 99.11%, respectively. The average runtime of single identification is 5.26 ms. It meets the technical requirements of household AFCI or AFDD.

INDEX TERMS Depthwise separable convolution, fault diagnosis, fault line selection, lightweight design, series arc fault.

I. INTRODUCTION

In household power supply lines, series arc fault (SAF) often occurs due to aging of insulation and poor contact. The temperature of the SAF is above 2000 °C, which can ignite the wire insulation or any other inflammable materials around the fault location in a very short time, causing a fire. SAF is one of the main causes of home fire accident [1]. When a SAF occurs, the root-mean-square of current is lower than that in normal state, which makes the conventional short-circuit, over-current and leakage current protection devices unable to accurately identify the fault and realize fault protection [2]. It is generally believed that the installation of arc fault circuit interrupter (AFCI) or arc fault detection device (AFDD) in electrical circuits is the most effective way to implement arc fault protection.

At present, the household AFCI or AFDD products on the market can only identify the SAF occurring in a single-branch circuit or in the main-circuit of a multi-branch circuit, and the identification accuracy needs to be further improved. However, a household power supply system contains many branch-circuits. These branch-circuits usually work simultaneously. A SAF may occur in each branch-circuit. If an AFCI or AFDD is installed in each branch-circuit, it will inevitably bring a series of problems such as the complexity of the distribution system, the increased size of the distribution box, and higher costs. Obviously, it is unreasonable, or at least it is inconvenient. In this case, it is very necessary to design a SAF identification method suitable for household multi-branch circuit, which can identify the SAF in each branch-circuit only by using the main-circuit current signal, and also has the

The associate editor coordinating the review of this manuscript and approving it for publication was Yongming Li.

function of fault line selection. It is of great significance for the development of AFCI or AFDD with the above functions and the prevention of home electrical fires.

A lot of research has been done on household SAF identification methods. Most of them identify the SAF by analyzing the current signals. Artale et al. [3] and Zhao et al. [4] selected the frequency-domain and time-domain indicators of the current signal, and used the threshold judgment method to detect the SAF. Jiang et al. [5] adopted a short-observation-window singular value decomposition and reconstruction algorithm to analyze the current signal and used thresholds to identify the SAF in residential buildings. Luan et al. [6] applied two time-domain features of the current signal and thresholds to detect the SAF. The time-domain features are absolute error between adjacent current cycles, and the zero current period of current signal, respectively. Guo et al. [7] calculated the time-domain and time-frequency domain features of current signals by wavelet packet decomposition and variational mode decomposition, and identified the SAF by using support vector machine (SVM). Qu et al. [8] extracted four time-domain features and ten frequency-domain features of current signals, and designed a SVM optimized by particle swarm optimization algorithm to detect the SAF. Zou et al. [9] constructed a highly identifiable features by combining sensitive current components and strong discriminative features, and used a standard SVM to identify the SAF. Ferracuti et al. [10] used textural image features extracted from gray-level co-occurrence matrix to represent the fault indicators, and exploited the recurrence quantification plots to detect the SAF. Wang et al. [11] proposed a signal preprocessing method based on the improved Mel Frequency Ceptral coefficient, and employed a fully connected neural network (FCNN) to identify the SAF. Wang et al. [12] converted the current signal into a series of sparse coefficients and then applied a FCNN to identify the SAF. Wang et al. [13] first determined the load category according to the fundamental frequency component of the current signal, and then took the specific time-domain and frequency-domain indicators as the input, and finally adopted different FCNNs to identify the SAF occurred in different types of load circuit. Dowalla et al. [14] presented a SAF detection and fault location method by analyzing both current and voltage signals. The random forest classifier and k-nearest neighbor algorithm were adopted respectively to realize the fault detection and fault location function. Jiang et al. [15] extracted two time-domain features by impulse factor analysis and covariance matrix analysis, and a frequency-domain feature by multiple frequency-band analysis, and then utilized a threshold and a SVM to detect the SAF. In [3], [4], [5], [6], [7], [8], [9], [10], [11], [12], [13], [14], and [15], the signal analysis methods, and the threshold method or traditional machine learning algorithms are combined to detect the SAF. Since we have to artificially determine the signal analysis method, construction method of the feature vectors, and classifier, the above methods have strong subjectivity. Moreover, when the load or circuit topology varies, the generality of these methods is poor.

Recently, several deep learning algorithms based domestic SAF identification methods have been proposed. Yang et al. [16] identified the SAF in multi-load circuit by using a temporal domain visualization convolutional neural network (CNN). Zhang et al. [17] first arranged the normalized current signals piecewise to obtain a two-dimensional (2-D) gray matrix, and then adopted a self-normalized CNN to identify the SAF. Zhou et al. [18] extracted morphological features of the current signals and designed a customized multi-scale CNN to detect the SAF. Zhang et al. [19] proposed an adaptive SAF identification model, and used generative adversarial networks to realize data enhancement function. Jiang et al. [20] selected the feature vectors of the SAF from the time-domain, frequency-domain features and wavelet packet energy indicators of current signals, and applied a deep neural network to identify the fault. Zhang et al. [21] first fused the multi-layer discrete wavelet details of the current signal into a matrix, then converted the matrix into a phase space image, and used a deep residual network to identify the SAF. Chu et al. [22] deployed a CNN to the embedded device Zynq-7020, and realized the on-line detection of the SAF occurred in household circuit. Paul et al. [23] designed a machine learning algorithm named Efficient-ArcNet to detect the SAF, and implemented it in Raspberry Pi 4B to verify the practicability of the method. Wang et al. [24] deployed a CNN to Raspberry Pi 3B to identify the SAF, and tested the performance of the network.

In [16], [17], [18], [19], [20], [21], [22], [23], and [24], although these methods have good identification performance and generalization performance, they still have the following shortcomings.

1) The methods in [16], [17], [19] and [21], [22], [23], and [24] are used to identify the SAF occurred in a single-branch circuit or in the main-circuit of a multi-branch circuit. However, a household power supply system has many branch-circuits, and usually multiple branch-circuits operate simultaneously. In the multi-branch circuit, the main-circuit current will be effected by the load type and the number of load in each branch-circuit. When SAF occurs in a branch-circuit, the main-circuit current includes both the arc fault current signal of the fault branch-circuit and the normal working current signals of all other normal branch-circuits. These normal working current signals will weaken or submerge the fault features of the SAF to a certain extent. It is very difficult to accurately identify the SAF occurred in the branch-circuit only by analyzing the main-circuit current signal, which contains weak SAF feature information. Therefore, whether the existing SAF identification method for a single-branch circuit can still be applied to household multi-branch circuit needs further verification.
2) The methods in [2], [7], [15], [18], and [20] are suitable for the identification of the SAF in the household multi-branch circuit. But they can only be implemented in computers, and the feasibility of implementation in

embedded microprocessors needs to be further tested. Up to now, the implementation of the fault identification and fault line selection method for the SAF in household multi-branch circuit in embedded microprocessors has not been reported.

3) Although the methods in [22], [23], and [24] have been implemented in embedded devices, they still have the following insufficiencies. The method in [22] requires a specially designed high-frequency coupling sensor to detect circuit current. The detection performance of the methods in [23] and [24] needs to be improved. In addition, the above methods do not consider the adaptability of the identification model to the signal sampling frequency. When the sampling frequency changes, the model structure needs to be adjusted and the model needs to be retrained. It is very inconvenient in practical application. Therefore, how to optimize the existing identification model so that it can run in a general-purpose embedded microprocessor is crucial for the development of intelligent and miniaturized AFCI or AFDD.

To solve the above problems, a CNN-based SAF identification model was proposed in this work. The main innovations and academic contributions are as follows.

1) A lightweight SAF identification model based on 1-D CNN was proposed to identify the SAF occurred in household multi-branch load circuit. The model can realize both fault identification and fault line selection functions of the SAF only by analyzing the main-circuit current signal. Moreover, it has strong adaptive ability to signal sampling frequency. It provides a new solution for the development of household AFCI or AFDD with the fault line selection function.
2) One-dimensional (1-D) depthwise separable convolution was used to optimize the identification model, which reduces the computational cost of feature extraction. The optimized model has lower complexity and is much easier to be implemented in embedded microprocessors.
3) The model was successfully deployed to the embedded device Jetson nano. Its accuracy and runtime were tested by the device, and its effectiveness was verified.

The rest of the article is organized as follows. Section II introduces the SAF experiments, and the creation of the dataset. Section III describes the details of the design and optimization of the SAF identification model. Section IV presents the hardware implementation of the model, and discusses the effectiveness of the model under different test conditions. Section V concludes this article.

II. SAF EXPERIMENTS AND DATASET CREATION

A. SAF EXPERIMENTS

A SAF generator was developed according to UL1699 standard, as shown in Fig. 1. It mainly consists of a static electrode, a movable electrode, a stepper motor, a sliding bench, an insulating basement, two insulating supports, wires,

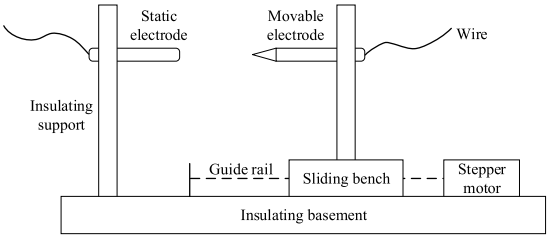

(a)

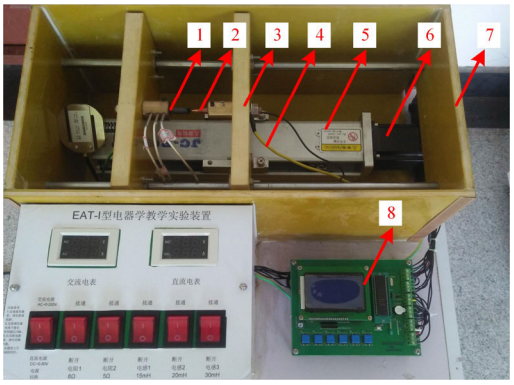

1- static electrode, 2-movable electrode, 3-insulating support, 4-wire, 5-sliding bench, 6-stepper motor, 7-insulating basement, 8-control circuit board

(b)

FIGURE 1. SAF generator. (a) Principle diagram. (b) Photo.

TABLE 1. Experimental loads and their parameters.

Branch-circuit	Load in the branch-circuit	Rated current (A)	Rated power (W)
L_1	Light bulb	0.91	200
L_2	Computer	1.14	250
L_3	Induction cooker	10.00	2200
L_4	Electric drill	2.64	580
L_5	Angle grinder	2.27	500
L_6	Hair drier	3.64	800

and a control circuit board. The movable electrode and static electrode are copper rod and carbon rod, respectively. The diameter of the two rods is 5mm. The static electrode is installed on the insulating basement through the insulating support. And the movable electrode is installed on the insulating support, which is fixed on the sliding bench. The stepper motor is used to control the reciprocating motion of the sliding bench, so as to adjust the position of the movable electrode. Here, the control of the stepper motor is achieved by using the control circuit board.

Using the SAF generator, six typical household appliances in Table 1 were selected as the experimental loads. According to Table 2, the SAF experiments were carried out in single-branch, two-branch, four-branch, and six-branch circuit, respectively.

The experimental circuit is shown in Fig. 2. A commercial AC power supply was used as the experimental power supply. Its rated output voltage is 220 V and its fundamental

TABLE 2. Experimental scheme.

Group No.	Used branch-circuit	Circuit type	Branch-circuit where the SAF occurs
S_1-S_6	L_1-L_6	Single-branch	L_1, L_2, L_3, L_4, L_5, L_6
S_7-S_8	L_1+L_3	Two-branch	L_1, L_3
S_9-S_{12}	L_1-L_4	Four-branch	L_1, L_2, L_3, L_4
S_{13}-S_{18}	L_1-L_6	Six-branch	L_1, L_2, L_3, L_4, L_5, L_6

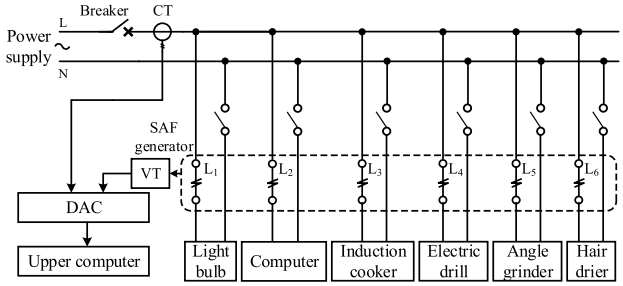

FIGURE 2. Diagram of the experimental circuit.

frequency is 50 Hz. The SAF in each branch-circuit can be simulated by connecting the SAF generator in series to the circuit.

According to the arc-drawn method, a SAF can be generated by controlling the reciprocating motion of the movable electrode of the SAF generator. The specific operation process is as follows. For each experiment, first connect the SAF generator to a branch-circuit in series, and make the movable and static electrodes of the SAF generator contact together. Then, power on the branch-circuit to make it run normally. Next, slowly adjust the position of the movable electrode by controlling the stepper motor installed in the SAF generator, and an arc is generated in the gap between the static and movable electrodes. In the arc burning stage, if the fluctuation of arc voltage and arc current is very small, the arc is considered to be approximately stable, that is, the arc is in quasi-stable burning state. When the arc is in quasi-stable burning state, stop adjusting the position of the movable electrode. During the arc burning process, the factors affecting the arc burning state are not changed deliberately. In this case, the arc will keep burning in the quasi-stable burning state. At this time, the main-circuit current signal and the voltage signal across the static and movable electrodes (i.e., arc voltage signal) are collected. If the arc extinguishes in the process of signal acquisition, immediately adjust the position of the movable electrode by controlling the stepper motor so as to re-generate an arc in quasi-stable burning state in the arc gap. In the data processing stage, the main-circuit current signal is selected according to the arc voltage signal, and only the main-circuit current signal when the arc is in quasi-stable state is used to create the SAF dataset. It should be noted that in household power supply lines, the occurrence of the SAF is random. In order to simulate the random characteristics of the occurrence of actual SAF as much as possible, the phase of the SAF in each current cycle is not specially set during the experiments.

During the experiment, an HCS-ES5 type hall current transformer (CT) was used to measure the main-circuit current signal. Its measuring range is 0-25 A, linearity is smaller than 0.1%, and response time is shorter than 1μs. An HVS-AS type hall voltage transformer (VT) was used to measure the voltage signal across the static and movable electrodes of the SAF generator. The voltage transformer has an internal measuring resistance of 50 Ω. Its rated input current is 5 mA, linearity is smaller than 0.1%, and response time is shorter than 40 μs. A USB-3200 type data acquisition card (DAC) was used to upload the current and voltage signals to a computer for subsequent data analysis. The DAC has a 12-bit analog-to-digital converter, and its maximum sampling frequency is 500 kHz. In this section, the sampling frequency of the current and voltage signals is 50 kHz.

B. ANALYSIS OF EXPERIMENTAL RESULTS

Fig. 3 shows the main-circuit current waveforms with or without SAF in different branch-circuits.

In normal state, i.e., there is no SAF in the multi-branch circuit, the main-circuit current waveform is a sine wave when the load of the branch-circuit is a light bulb, induction cooker, and hair dryer, respectively. When the load is an angle grinder, the current waveform is a triangular wave. When the load is an electric drill, there are a few low amplitude burrs in the current waveform. When the load is a computer, there is obvious ''flat shoulder'' phenomenon in the current waveform, which is similar to the main-circuit current waveform when a SAF occurs in the light bulb, electric drill, angle grinder, or hair dryer branch-circuit. So it is easy to cause misjudgment in identifying the SAF.

In arc fault state, i.e., a SAF occurs in any branch-circuit, there are different degrees of ''flat shoulder'' phenomenon and burrs in the main-circuit current waveform. Compared with that in the hair dryer branch-circuit, the ''flat shoulder'' phenomenon in the main-circuit current waveform is more obvious when the SAF occurs in the light bulb or angle grinder branch-circuit. This is because the rated current of the above three loads is different, which leads to the different arcing intensity when the SAF occurs. In addition, when the SAF occurs in different branch-circuits, the characteristics of burrs in the current waveform are obviously different. The main difference are as follows. In the light bulb or angle grinder branch-circuit, burrs appear at the edge of the ''flat shoulder'' position in the current waveform. In the computer branch-circuit, a great deal of burrs is concentrated in the ''flat shoulder'' position in the current waveform. In the induction cooker branch-circuit, burrs appear near the peak and trough of the current waveform. In the electric drill branch-circuit, burrs appear at the edge of the ''flat shoulder'' position, as well as near the peak and trough of the current waveform. Furthermore, the amplitude of the burrs at the edge of the ''flat shoulder'' position is much higher than that at other positions. Different from the random burr generated by electromagnetic

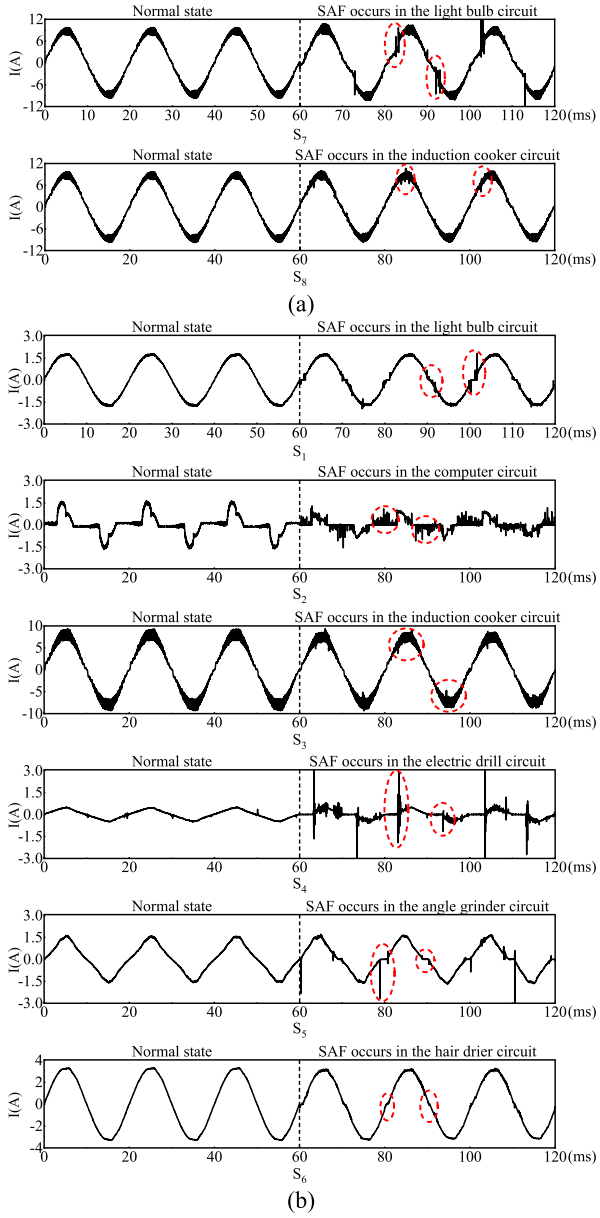

FIGURE 3. Main-circuit current waveforms with and without SAF. (a) Two-branch circuit. (b) Six-branch circuit.

interference, the above burr characteristics have certain regularity. Therefore, making full use of the above waveform features will help to reduce misjudgment and improve the identification accuracy.

When multiple branch-circuits operate in parallel, the amplitude of the main-circuit current is larger than that of branch-circuit. If a branch-circuit current is very small, the signal features generated by the SAF in the branch-circuit may be weakened or submerged by the main-circuit current signal, which makes it more difficult to identify the SAF in multi-branch circuit. To address this issue, convolutional neural network was used in this article to identify the SAF in this application scenario.

TABLE 3. Distribution of fault samples.

Branch-circuit	Load in the branch-circuit	Source of sample data	Number of sample
L_1	Light bulb	S_1, S_7, S_9, S_{13}	32154
L_2	Computer	S_2, S_{10}, S_{14}	17035
L_3	Induction cooker	S_3, S_8, S_{11}, S_{15}	23385
L_4	Electric drill	S_4, S_8, S_9	14980
L_5	Angle grinder	S_5, S_{17}	11335
L_6	Hair drier	S_6, S_{18}	8138

C. DATASET CREATION

To retain the complete feature information of current waveform in the sample data, the samples were intercepted from the measured main-circuit current signals and used as the input of the SAF identification model. The size of input sample will affect the accuracy and complexity of the identification model. Under the same conditions, the more sampling points in each sample, the more effective information it contains, the higher the identification accuracy, and accordingly, the higher the time complexity and space complexity of the model. Therefore, it is necessary to select the most appropriate number of sampling points for the data samples. When the sampling frequency is 50 kHz, there are a total of 1000 sampling points in each current cycle. The test results showed that when the number of sampling points for each sample is 700, that is, the current waveform with 70% current cycle length is taken as a sample, the complexity and accuracy of the identification model described in Section III-A are well balanced. As seen in Fig. 3, when the SAF occurs in a branch-circuit, the waveform features of the main-current mainly appear at the ''flat shoulder'' position, and near the peak and trough of the waveform. Therefore, when each sample contains 700 sampling data, the sample contains the main feature information of the circuit waveform.

The original data of the measured main-current signal was divided by 700 sampling points, and a total of 159794 data samples were obtained. Among them, there are 52767 normal samples and 107027 fault samples. Fault samples come from six different branch-circuits, and the specific distribution is shown in Table 3. The category label of normal sample was set as 0, and the category labels of fault sample from L_1 to L_6 branch-circuits were set as 1, 2, 3, 4, 5, and 6, respectively. The sample dataset of the SAF was finally obtained. According to the category label output by the identification model, it can determine whether there is a SAF in the circuit and the branch-circuit where the fault occurs. In this way, the fault identification and fault line selection functions can be realized.

4000 samples were randomly taken from the normal samples of the dataset, and 4000 fault samples were randomly taken from each branch-circuit of L_1-L_6 to form a new dataset, defined as Dataset2. The remaining samples in the dataset were defined as Dataset1. In Dataset1, 80% of the samples were used as train samples, and 20% of them were used as test samples. Dataset1 was used to train and test

TABLE 4. Specific parameters of DtNet.

Layer	Activation	Kernel	Padding	Stride
1-D S-Conv layer	Relu	3,32	valid	1
1-D Pooling layer	-	-	valid	2
1-D S-Conv layer	Relu	3,64	valid	1
1-D Pooling layer	-	-	valid	2
1-D S-Conv layer	Relu	3,128	valid	1
1-D Pooling layer	-	-	valid	2
1-D S-Conv layer	Relu	3,256	valid	1
1-D Pooling layer	-	-	valid	2
Flatten	-	-	-	-
Dense	Relu	256,1	-	-
Dense	Softmax	7,1	-	-

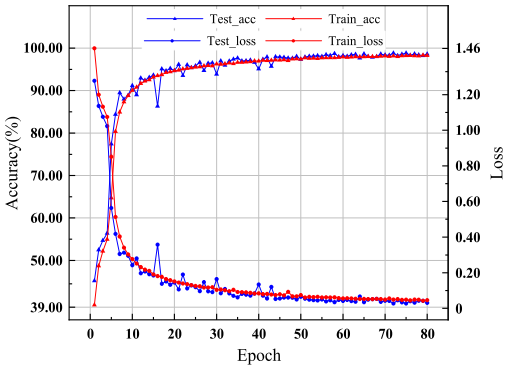

FIGURE 4. Accuracy and loss of DtNet.

the identification model on the computer. It was also used to adjust the hyper-parameters of the SAF identification model so as to achieve the lightweight design of the model. In essence, the test set in Dataset1 is a so-called validation test. Dataset2 was pre-loaded into the embedded device introduced in Section IV-A and used to off-line test the performance of the identification model. So Dataset2 is a true test set used to test the generalization performance of the model.

III. SAF IDENTIFICATION MODEL

A. CREATION OF THE IDENTIFICATION MODEL

The input of 1-D CNN is a 1-D vector. Compared with two-dimensional CNN and three-dimensional CNN, it has smaller time complexity and space complexity, and is easier to run in embedded devices. Therefore, a SAF identification model DtNet based on 1-D CNN was designed in this section.

DtNet consists of a data pre-processing module, a feature extraction module and a feature calculation module. The data pre-processing module is used to perform maximum and minimum normalization to the data samples, so as to exclude the influence of different working current and accelerate the convergence speed of the model training. The feature extraction module consists of 1-D convolutional layers and 1-D maximum pooling layers. The module is used to extract data features from the data samples, and encode each data sample into 256 channel high-level features. The feature calculation module is used to further calculate the extracted features by using a FCNN with a hidden layer, and then output the identification results by the output layer of the identification model. There are 7 neurons in the output layer, corresponding to category labels 0-6, respectively. These labels respectively represent 7 operation states of the circuit, i.e., normal state, SAF occurs in the light bulb, computer, induction cooker, electric drill, angle grinder, and hair drier branch-circuit.

The convolution kernel size of DtNet is 3, the stride is 1 by default, and the padding is set as valid. In order to make DtNet have the ability of nonlinear expression, so as to better learn data samples, the Relu activation function was introduced into both feature extraction module and feature calculation module. The specific parameters of DtNet are shown in Table 4. In Table 4, S-Conv is short for standard convolution.

DtNet was trained by using the train set of Dataset1. The key parameter settings are as follows. The batch size is set as 32, the epoch is 80, and the optimizer uses Adam algorithm. Considering the category labels are integer data, sparse cross-entropy function was used to evaluate the loss between the predicted values of the identification model and truth labels. After the DtNet was trained, its identification accuracy was tested by using the test set of Dataset1. As shown in Fig. 4, the identification accuracy of DtNet on both train set and test set is higher than 98% after the 68th epoch. It shows that the trained DtNet can meet the accuracy requirements of identifying SAF.

B. LIGHTWEIGHT DESIGN OF THE MODEL

At present, the difficulty in the application of the SAF identification models based on deep learning algorithms in industrial microprocessors is mainly reflected in the contradiction between the high time and space complexity of identification models and the low computational capability and storage performance of microprocessors. To solve the above problem, it is necessary not only to improve the performance of the microprocessors, but also to carry out lightweight design of the identification model. The model can be optimized from the perspective of reducing its floating point operations (FLOPs) and memory access cost (MAC), so as to reduce its complexity and finally realize the hardware deployment of the model.

Depthwise separable convolution (DS-Conv) can reduce the computational cost of feature extraction through the combination of depthwise convolution (DW-Conv) and pointwise convolution (PW-Conv).

Taking the size of the input feature map as $10 \times 10 \times 3$ and the size of the output feature map as $8 \times 8 \times 5$ as an example, the standard convolution and depthwise separable convolution in Fig. 5 were respectively used for calculation. If the size of the standard convolution kernel and the depthwise convolution kernel are both 3×3, the FLOPs and MAC required to complete the above operation are shown in Table 5. The FLOPs and MAC of standard convolution are calculated by (1) and (2), respectively. For depthwise separable convolution, the FLOPs of each kernel in the depthwise

TABLE 5. Comparison between standard convolution and depthwise separable convolution.

Layer	Size of input operators	Size of output operators	FLOPs	MAC (Byte)
S-Conv layer	10×10×3	8×8×5	17280	3040
DS-Conv layer	10×10×3	8×8×5	5376	4216

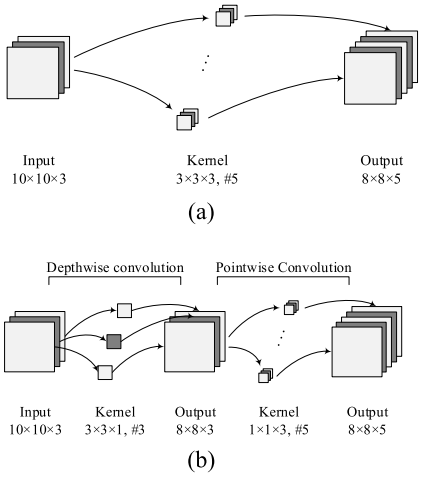

FIGURE 5. Standard convolution (S-Conv) and depthwise separable convolution (DS-Conv). (a) S-Conv. (b) DS-Conv.

convolution is calculated separately according to (1), and the FLOPs of pointwise convolution is calculated according to (1). The MAC of depthwise convolution and pointwise convolution is calculated according to (2).

$$F = 2 \cdot M_l^2 \cdot K_l^2 \cdot C_{l-1} \cdot C_l \tag{1}$$

$$M = [M_{l-1}^2 \cdot C_{l-1} + (K_l^2 \cdot C_{l-1} + 1) \cdot C_l + M_l^2 \cdot C_l] \times S \tag{2}$$

where, F represents FLOPs. It is the number of floating point operations performed for a forward propagation of a model or an operator. M represents the MAC, which is the size of the memory unit that the model or operator needs to access during the operation. The unit of MAC is Bytes. M_{l-1} and M_l are respectively the size of the input and output feature map of the convolution operator. C_{l-1} and C_l are respectively the number of the input and output channels of the convolution operator. K_l is the size of the convolution kernel of the operator. If the type of operation data is float32, the variable S in (2) is 4.

As seen in Table 5, when the depthwise separable convolution is used instead of the standard convolution, the MAC increases slightly, but the FLOPs decreases significantly. Obviously, it is beneficial to reduce the time complexity of the identification model.

To simplify the time complexity of DtNet and achieve its lightweight design, the second, third and fourth convolutional layers in the feature extraction module of DtNet were improved by using depthwise separable convolution. Moreover, in order to accelerate the convergence speed of the improved identification model, batch normalization layers (BN) were introduced in the header of the model, and at the back of both convolutional layers and fully connected layers. The optimized DtNet was labeled as Li-DtNet. The overall structure of Li-DtNet is shown in Fig. 6.

TABLE 6. Comparison between DtNet and Li-DtNet.

Identification Model	FLOPs	MAC (MByte)	Space (MByte)	Accuracy (%)
DtNet	34.63	12.43	32.2	98.71
Li-DtNet	16.02	13.53	31.4	99.23

According to the method of training and testing DtNet, Li- DtNet was trained and tested by using the train set and test set of Dataset1, respectively. Then, the accuracy and loss of Li-DtNet were tested. As shown in Fig. 7, the identification accuracy of Li-DtNet on both train set and test set is higher than 99% after the 52th epoch. It indicates that the trained Li-DtNet can meet the accuracy requirements of identifying SAF.

The performance indicators of DtNet and Li-DtNet were statistically analyzed. The comparison results are shown in Table 6. In Table 6, space refers to the size of the computer disk space occupied by the model file. Accuracy refers to the accuracy of the model on the test set of Dataset1. Table 6 shows that Li-DtNet has a higher accuracy than DtNet. Although the MAC of Li-DtNet increases slightly, the FLOPs of Li-DtNet decreases significantly, which is only 46.26% of that of DtNet. So Li-DtNet achieves the lightweight of DtNet and has better comprehensive performance. Li-DtNet can be deployed to industrial microprocessors to identify the SAF.

IV. HARDWARE IMPLEMENTATION AND PERFORMANCE TEST OF LI-DTNET

A. IMPLEMENTATION OF LI-DTNET IN AN EMBEDDED DEVICE

The model Li-DtNet was deployed to the embedded device Jetson nano shown in Fig. 8. Jetson nano mainly consists of a Quad-Core Cortex-A57 ARM processor, a 128-core NVIDIA Maxwell GPU and a 4GB 64-bit LPDDR4. It also has GPIO, USB3.0 and other ports.

The model file of Li-DtNet is firstly converted to tflite format file by using the TFLite converter in computer, and downloaded to the embedded device. Then the model runs in the embedded device through the TFLite interpreter, so as to realize the inference and identification of data samples.

B. PERFORMANCE TEST OF LI-DTNET RUNNING IN THE EMBEDDED DEVICE

The real-time performance and identification accuracy of Li-DtNet were tested off-line in Jetson nano. Li-DtNet first reads the data samples in Dataset2, which are pre-loaded into the device, and then performs the inference identification. The performance of Li-DtNet running in the embedded

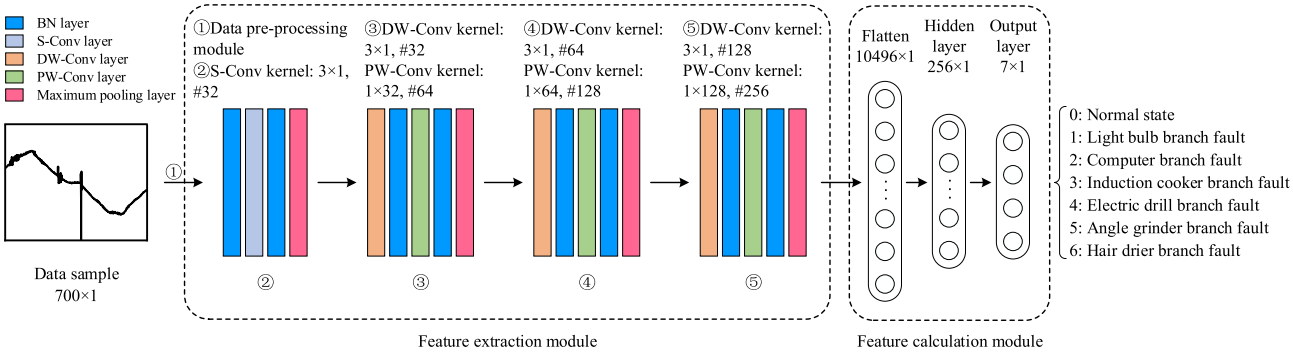

FIGURE 6. Overall structure of Li-DtNet.

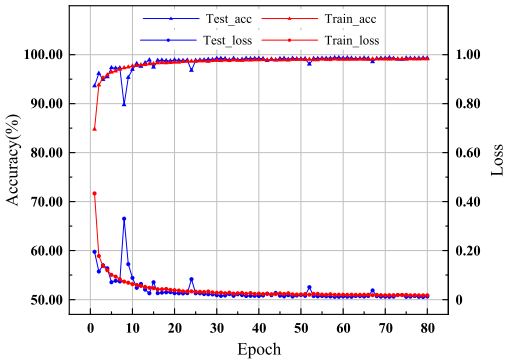

FIGURE 7. Accuracy and loss of Li-DtNet.

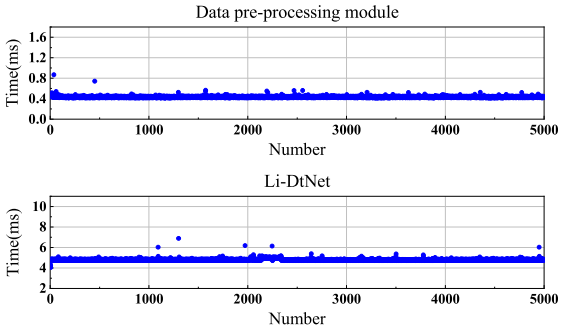

FIGURE 9. Test results of the runtime.

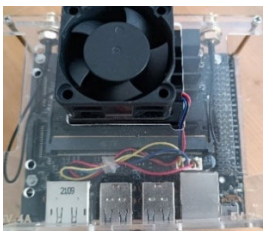

FIGURE 8. Photo of Jetson nano.

device can be evaluated by analyzing statistically its runtime and accuracy.

The runtime of the data pre-processing module and Li-DtNet was respectively tested for 5000 times. The test results are shown in Fig. 9. As seen in Fig. 9, the average runtime of the data pre-processing module is 0.45 ms, and the average runtime of Li-DtNet is 4.81 ms. It means that the average runtime of identifying a sample is 5.26 ms. According to IEC62606 standard [25], in AC 230 V system, the maximum allowable break time for the SAF in 5 A load circuit is 500 ms. The maximum allowable break time for the SAF in 63 A load circuit is 120 ms. In this case, when the SAF is identified by Li-DtNet, the fault circuit can be disconnected within the maximum break time specified in the above standards even if the ordinary household circuit breaker is used to break the circuit. Therefore, the real-time performance of Li-DtNet running in the embedded device meets the technical requirements of developing AFCI or AFDD.

Li-DtNet was used to identify the data samples in Dataset2, and the identification results are shown in Fig. 10. Fig. 10 shows that Li-DtNet can accurately judge whether there is a SAF or not in the circuit, and the identification accuracy of SAF is 100%. When the SAF occurs in the light bulb, induction cooker, and angle grinder branch-circuit, there are 5, 1, and 2 misjudgments of the branch-circuit where the fault is located, respectively. That is, when the SAF occurs in the branch-circuit from L_1 to L_6, the accuracy of fault line selection is 99.88%, 100%, 99.98%, 100%, 99.95% and 100%, respectively, and the average accuracy of fault line selection is 99.97%. In our opinion, the reasons for the SAF misclassification of Li-DtNet are as follows: a) Under the influence of circuit parameters, load type, arc burning environment and other factors, the burning state of AC SAF in the circuit changes instantaneously, which leads to the components of the current signal are very complicated and variable. This is one of the main reasons for SAF misjudgment. b) As seen in Fig.3, when a SAF occurs in any branch-circuit, there are different degrees of "flat shoulder" phenomenon and burrs in the main-circuit current waveform. So the main-circuit current waveforms in fault state have a certain degree of similarity. In addition, when the burning state of the arc fault is different, even for the same load circuit, the arc resistance of the SAF is also different, which leads to a certain difference

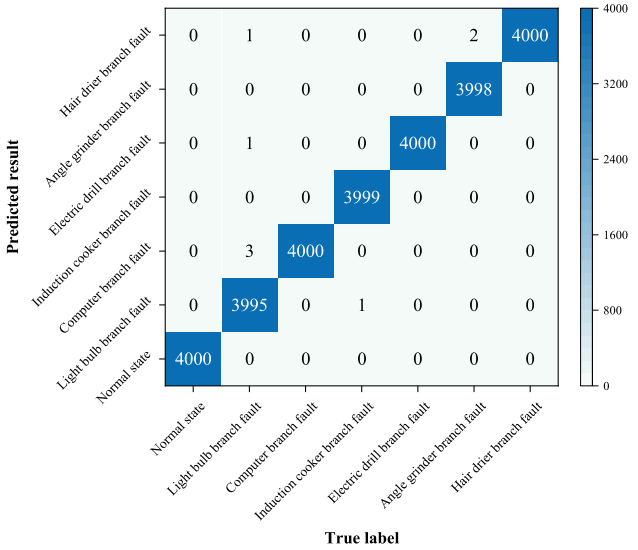

FIGURE 10. Test results of fault identification and fault line selection.

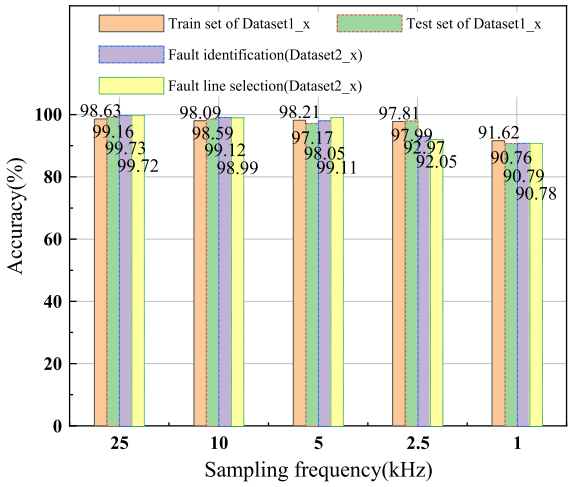

FIGURE 11. Test results at different sampling frequencies.

in the amplitude attenuation of fault current waveform and the distortion degree of the waveform (such as the strength of the flat shoulder and the number of burrs). This difference may increase the similarity of main-circuit current waveforms between different branch-circuits to a certain extent, thus increasing the probability of SAF misjudgment. c) When multiple branch-circuits operate in parallel, if a branch-circuit current is very small, the signal features generated by the SAF in the branch-circuit may be weakened or submerged by the main-circuit current signal. It will also increase the probability of SAF misjudgment.

Fig. 10 shows that when Li-DtNet runs in the embedded device, the accuracy of fault identification and fault line selection of the SAF can meet the detection accuracy requirements of AFCI or AFDD.

C. VALIDATION TEST OF LI-DTNET UNDER OTHER CONDITIONS

1) VALIDITY OF LI-DTNET UNDER THE CONDITION OF LOWER SIGNAL SAMPLING FREQUENCY

The sampling frequency of current signal may lower than 50 kHz in engineering application. Lowering the sampling frequency of the current signal will inevitably reduce the data sample quality, and then directly affect the identification accuracy of the model. Therefore, it is necessary to carry out the validity test of Li-DtNet under the condition of lower sampling frequency.

The accuracy of Li-DtNet was tested off-line with the embedded device at the sampling frequencies of 1 kHz, 2.5 kHz, 5 kHz, 10 kHz and 25 kHz. First, Dataset1 and Dataset2 were down-sampled with the above five sampling frequencies, respectively. The corresponding datasets were obtained, and labeled as Dataset1_x and Dataset2_x. Where, x represents the categories of the above five sampling frequencies, x=1, 2.5, 5, 10, 25. For example, Dataset1_1 is the dataset obtained by down-sampling Dataset1 at the frequency of 1 kHz. Second, the linear interpolation method was introduced in the data pre-processing module to up-sample the above down-sampled data samples, so that each data sample is a vector with the size of 700 × 1. Then, according to the method of training and testing DtNet, Li-DtNet was trained and tested by using Dataset1_x. The trained Li-DtNet was deployed to Jetson nano. Finally, the accuracy of Li-DtNet was tested. The test results are shown in Fig. 11.

Fig. 11 shows that when the signal sampling frequency is lowered, the accuracy of the fault identification and fault line selection of the SAF does decrease to different degrees. However, even when the sampling frequency is lowered to 1 kHz, the accuracy of the fault identification and fault line selection can still reach more than 90%, which indicates that Li-DtNet has strong adaptability to signal sampling frequency.

When the sampling frequency is lower than 5 kHz, the accuracy of Li-DtNet decreases rapidly. Therefore, it is recommended that the sampling frequency of the current signal should not be less than 5 kHz. In this case, both the accuracy of the fault identification and the accuracy of the fault line selection are higher than 98%, which can meet the detection accuracy requirements of AFCI or AFDD.

2) VALIDITY OF LI-DTNET UNDER DIFFERENT LOAD TYPES AND CIRCUIT TOPOLOGIES CONDITIONS

In order to evaluate the validity of Li-DtNet when the load type or circuit topology changes, additional SAF experiments were carried out in single-branch, two-branch, and three-branch circuits by using the loads in Table 7. The experimental scheme is shown in Table 8. The experimental circuit is shown in Fig. 12. During the experiments, the signal sampling frequency is 25 kHz.

A total of 85570 data samples were obtained by intercepting the measured main-circuit current signal with the length of a current cycle as an interval. Among them, there are 21344 normal samples and 64226 fault samples. Fault

TABLE 7. Experimental loads and their parameters.

Branch circuit	Load in the branch-circuit	Rated current (A)	Rated power (W)
L_{t1}	Floor fan	0.25	56
L_{t2}	Electric blanket	0.27	60
L_{t3}	Computer	1.00	220

TABLE 8. Experimental scheme II.

Group No.	Used branch-circuit	Circuit type	Branch-circuit where the SAF occurs
S_{t1}-S_{t3}	L_{t1}-L_{t3}	Single-branch	L_{t1}, L_{t2}, L_{t3}
S_{t4}-S_{t5}	L_{t1}+L_{t2}	Two-branch	L_{t1}, L_{t2}
S_{t6}-S_{t7}	L_{t1}+L_{t3}	Two-branch	L_{t1}, L_{t3}
S_{t8}-S_{t9}	L_{t2}+L_{t3}	Two-branch	L_{t2}, L_{t3}
S_{t10}-S_{t12}	L_{t1}-L_{t3}	Three-branch	L_{t1}, L_{t2}, L_{t3}

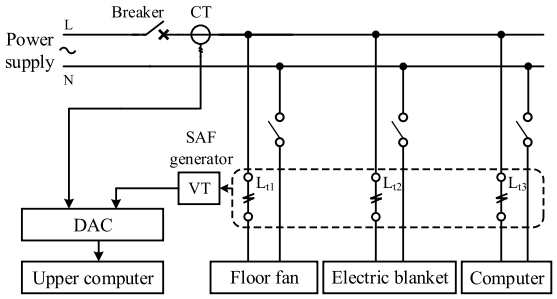

FIGURE 12. Experimental circuit after replacing the loads.

TABLE 9. Distribution of fault samples in Dataset3.

Branch-circuit	Load in the branch-circuit	Source of sample data	Number of sample
L_{t1}	Floor fan	S_{t1}、S_{t4}、S_{t6}、S_{t10}	21393
L_{t2}	Electric blanket	S_{t2}、S_{t5}、S_{t8}、S_{t11}	21866
L_{t3}	Computer	S_{t3}、S_{t7}、S_{t9}、S_{t12}	20967

samples come from 3 different branch-circuits, and the specific distribution is shown in Table 9. The category label of normal sample was set as 0, and the category labels of fault sample from L_{t1} to L_{t3} branch-circuits were set as 1, 2, and 3, respectively. The above sample dataset was obtained and labeled as Dataset3. According to the proportion of 80% and 20%, Dataset3 was divided into train set and test set.

When the sampling frequency is 25 kHz, each current cycle contains 500 sampling points. Therefore, the input size of Li-DtNet was set to 500 × 1. Since only four types of data samples need to be identified at this time, the output layer of Li-DtNet used four neurons to represent the following four operation states of the circuit, namely, normal state, SAF occurs in the floor fan branch-circuit, SAF occurs in the electric blanket branch-circuit, and SAF occurs in the computer branch-circuit.

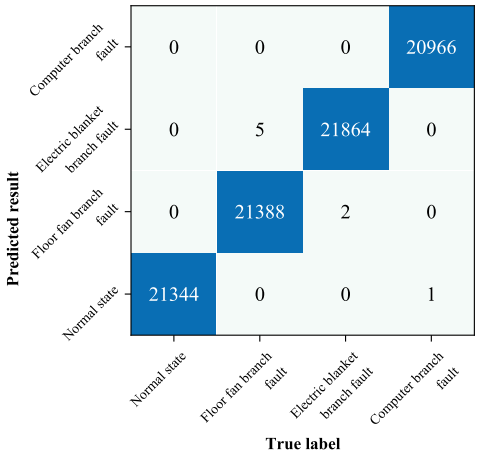

FIGURE 13. Test results after changing the load type and circuit topology.

According to the method of training and testing DtNet, Li-DtNet was trained and tested by using Dataset3. The test results of Li-DtNet running in Jetson nano are shown in Fig. 13. Fig. 13 shows that the accuracy of SAF identification and fault line selection of Li-DtNet is 99.9988% and 99.9875%, respectively, even when the load type and circuit topology are changed. So Li-DtNet has strong adaptability to load type and circuit topology.

D. COMPARISON WITH EXISTING METHODS

The performance of Li-DtNet was comprehensively evaluated from the aspects of identification principle, signal sampling frequency, identification accuracy and real-time performance in an embedded device.

The evaluation results were compared with similar methods in literatures [17], [22], and [24]. The comparison results are shown in Table 10.

As seen in Table 10, among these four methods, SCNN does not have the function of fault line selection. Whether the model can operate in embedded devices and its real-time performance need further test and verification. HCCNN needs to be equipped with a specially designed high-frequency coupled current sensor, and its signal sampling frequency is 1 MHz, which obviously put forward higher requirements for the engineering implementation of this model. Compared with ArcNet, which has better overall performance, Li-DtNet has the following advantages. a) It has better adaptability to signal sampling frequency. In the actual application process, when the sampling frequency of the current signal needs to be changed, the structure of Li-DtNet does not need to be readjusted, so as to improve the convenience of the application of the model. b) The average runtime of Li-DtNet is about 1/6 of that of ArcNet, so the real-time performance of Li-DtNet is better. c) The accuracy of fault identification and fault line selection of Li-DtNet is further improved, reaching 100% and 99.97%, respectively. Therefore, from the perspective of engineering application, Li-DtNet is more suitable for the development of AFCI or AFDD.

TABLE 10. Comparison between Li-DtNet and existing methods.

Methods	HCCNN[22]	SCNN[17]	ArcNet[24]	Li-DtNet（ours）
Identification principle	Specially designed high frequency CT + gray level image of current signal + 2-D CNN	Gray level image of current signal + self-normalization CNN	Original current signal + 1-D CNN	Original current signal + linear interpolation + lightweight 1-D CNN
Sampling frequency	1 MHz	102.4 kHz	10 kHz	1 kHz-50 kHz, Recommended≥5 kHz
Load type	Resistive, inductive, capacitive, and switching load	Resistor, resistor-inductance, and resistor-capacitance load	Resistors, motors, power electronic load, and gas discharge lamp load	Resistive, inductive, and switching load
Fault identification accuracy	99.20%	99.67%	99.47%	100%
Fault line selection function	Yes	No	Yes	Yes
Fault line selection accuracy	97%	-	99.05%	99.97%
Used embedded device	Zynq-7020	-	Raspberry Pi 3B	Jetson nano
Runtime in the embedded device	11 ms	-	31 ms	5.26 ms

TABLE 11. Test scheme for comparison between Li-DtNet and AFDDs.

Group No.	Used branch-circuit	Used AFDD	Branch-circuit where the SAF occurs
N_1	$L_{t1}+L_{t2}$	AFDD1	L_{t1}
N_2	$L_{t1}+L_{t2}$	AFDD1	L_{t2}
N_3	$L_{t1}+L_{t2}$	AFDD2	L_{t1}
N_4	$L_{t1}+L_{t2}$	AFDD2	L_{t2}

TABLE 12. Test results for comparison between Li-DtNet and AFDDs.

Group No.	Used AFDD	Action numbers of AFDD	Identification accuracy of Li-DtNet (%)
N_1	AFDD1	0	99.57
N_2	AFDD1	0	99.45
N_3	AFDD2	0	99.41
N_4	AFDD2	0	99.53

E. COMPARISON WITH AFDD PRODUCTS

To further evaluate the effectiveness of Li-DtNet, additional performance comparison tests were conducted between Li-DtNet and two household AFDD products. The J1AFDD-63C16 type AFDD and XM-AFD type AFDD were used in the tests. They are labeled as AFDD1 and AFDD2, respectively.

The comparison tests were carried out in a two-branch circuit. The branch-circuits L_{t1} and L_{t2} in Table 7 were used. The SAF generator shown in Fig.1 was connected in series to L_{t1} or L_{t2} branch-circuit to simulate the occurrence of the SAF in a particular circuit. AFDD1 or AFDD2 was installed in the main-circuit of the two-branch circuit. It was used to detect the SAF occurred in the branch-circuit. The main-circuit current signal was measured by using an HCS-ES5 type current transformer, and the voltage signal across the SAF generator was measured by using an HVS-AS type voltage transformer. The sample frequency is 50kHz. The test scheme is shown in Table 11.

Taking group No. N_1 in Table 11 as an example, the specific test process is as follows.

a) Power on the test circuit to make branch-circuits L_{t1} and L_{t2} work normally.

b) Control the SAF generator in the L_{t1} branch-circuit to repeatedly generate 50 SAFs in the branch-circuit. And the duration of each SAF is about 2s. At the same time, the main-circuit current and the voltage across the SAF generator are collected synchronously.

c) Count the action (alarm or trip) numbers of AFDD1 during the above 50 SAF occurrences.

d) Process the current and voltage data collected during the above 50 SAF occurrences according to the method in Section II-C, and obtain the test dataset of N_1.

e) Train Li-DtNet with the data samples obtained under S_{t4}-S_{t5} conditions in Table 8. Then, test the identification accuracy of trained Li-DtNet with the test dataset of N_1.

According to the above process, comparison tests were performed under N_1-N_4 conditions in Table 11. The test results are shown in Table 12. Under the test conditions of N_1-N_4, neither AFDD1 nor AFDD2 acted on the SAF that occurred on the branch-circuits of L_{t1} and L_{t2}. While the identification accuracy of Li-DtNet is higher than 99.451% under the same test conditions. So the identification accuracy of Li-DtNet is significantly better than that of these existing AFDD products.

V. CONCLUSION

In this paper, a SAF identification model Li-DtNet was designed based on lightweight 1-D CNN and successfully deployed in an embedded device. The fault identification and fault line selection functions of the SAF in multi-branch circuits can be realized in an embedded microprocessor only by detecting the main-circuit current. When Li-DtNet runs

in the embedded device, the average runtime of identifying a sample is 5.26 ms. Li-DtNet has the ability to adapt to the sampling frequency of the current signal by using linear interpolation method. When the sampling frequency is not less than 5 kHz, both the fault identification accuracy and fault line selection accuracy of SAF are higher than 98%.

Compared with similar methods, Li-DtNet has better real-time performance, higher identification accuracy and better adaptability to signal sampling frequency when running in the embedded device. It can be used to develop intelligent and miniaturized household AFCI or AFDD.

At present, the Jetson nano costs more than similar embedded devices such as the Raspberry Pi. From the perspective of reducing the cost of household AFCI or AFDD, one of the important works in the future is to further optimize Li-DtNet, so that it can be used in embedded devices with lower hardware cost without reducing the detection performance.

REFERENCES

[1] T. Yin and R. He, "Arc fault circuit interrupter," in *Low Voltage Electrical Apparatus Technical Manual*. Beijing, China: China Mach. Press, 2014, pp. 495–496.
[2] R. Jiang and Y. Zheng, "Series arc fault detection using regular signals and time-series reconstruction," *IEEE Trans. Ind. Electron.*, vol. 70, no. 2, pp. 2026–2036, Feb. 2023.
[3] G. Artale, A. Cataliotti, V. Cosentino, D. Di Cara, S. Nuccio, and G. Tinè, "Arc fault detection method based on CZT low-frequency harmonic current analysis," *IEEE Trans. Instrum. Meas.*, vol. 66, no. 5, pp. 888–896, May 2017.
[4] H. Zhao, H. Qin, and K. Liu, "A series fault arc detection method based on the fusion of correlation theory and zero current feature," *Chin. J. Sci. Instrum.*, vol. 41, no. 5, pp. 218–228, Apr. 2020.
[5] R. Jiang, G. Bao, Q. Hong, and C. D. Booth, "A coupling method for identifying arc faults based on short-observation-window SVDR," *IEEE Trans. Instrum. Meas.*, vol. 70, pp. 1–10, 2021.
[6] W. Luan, J. Lin, B. Liu, and B. Zhao, "Arc fault detection and identification via non-intrusive current disaggregation," *Electr. Power Syst. Res.*, vol. 210, Sep. 2022, Art. no. 108113.
[7] F. Guo, H. Gao, Z. Wang, J. You, A. Tang, and Y. Zhang, "Detection and line selection of series arc fault in multi-load circuit," *IEEE Trans. Plasma Sci.*, vol. 47, no. 11, pp. 5089–5098, Nov. 2019.
[8] N. Qu, J. Zuo, J. Chen, and Z. Li, "Series arc fault detection of indoor power distribution system based on LVQ-NN and PSO-SVM," *IEEE Access*, vol. 7, pp. 184020–184028, 2019.
[9] G. Zou, G. Fu, B. Han, W. Wang, and C. Liu, "Series arc fault detection based on dual filtering feature selection and improved hierarchical clustering sensitive component selection," *IEEE Sensors J.*, vol. 23, no. 6, pp. 6050–6060, Mar. 2023.
[10] F. Ferracuti, P. Schweitzer, and A. Monteric, "Arc fault detection and appliances classification in AC home electrical networks using recurrence quantification plots and image analysis," *Electr. Power Syst. Res.*, vol. 201, Dec. 2021, Art. no. 107503.
[11] Y. Wang, D. Sheng, H. Hu, K. Han, J. Zhou, and L. Hou, "A novel series arc fault detection method based on mel-frequency cepstral coefficients and fully connected neural network," *IEEE Access*, vol. 10, pp. 97983–97994, 2022.
[12] Y. Wang, F. Zhang, and S. Zhang, "A new methodology for identifying arc fault by sparse representation and neural network," *IEEE Trans. Instrum. Meas.*, vol. 67, no. 11, pp. 2526–2537, Nov. 2018.
[13] Y. Wang, F. Zhang, X. Zhang, and S. Zhang, "Series AC arc fault detection method based on hybrid time and frequency analysis and fully connected neural network," *IEEE Trans. Ind. Informat.*, vol. 15, no. 12, pp. 6210–6219, Dec. 2019.
[14] K. Dowalla, P. Bilski, R. Łukaszewski, A. Wójcik, and R. Kowalik, "A novel method for detection and location of series arc fault for non-intrusive load monitoring," *Energies*, vol. 16, no. 1, p. 171, Dec. 2022.
[15] R. Jiang, G. Bao, Q. Hong, and C. D. Booth, "Machine learning approach to detect arc faults based on regular coupling features," *IEEE Trans. Ind. Informat.*, vol. 19, no. 3, pp. 2761–2771, Mar. 2023.
[16] K. Yang, R. Chu, R. Zhang, J. Xiao, and R. Tu, "A novel methodology for series arc fault detection by temporal domain visualization and convolutional neural network," *Sensors*, vol. 20, no. 1, p. 162, Dec. 2019.
[17] T. Zhang, H. Wang, and R. Zhang, "An arc fault detection method based on the self-normalized convolutional neural network," *Chin. J. Sci. Instrum.*, vol. 42, pp. 141–149, Mar. 2021.
[18] G. Zhou, L. Huang, Z. Li, H. Tian, B. Zhang, M. Fu, Y. Feng, and C. Huang, "Intever public database for arcing event detection: Feature analysis, benchmark test, and multi-scale CNN application," *IEEE Trans. Instrum. Meas.*, vol. 70, pp. 1–15, 2021.
[19] T. Zhang, R. Zhang, H. Wang, R. Tu, and K. Yang, "Series AC arc fault diagnosis based on data enhancement and adaptive asymmetric convolutional neural network," *IEEE Sensors J.*, vol. 21, no. 18, pp. 20665–20673, Sep. 2021.
[20] J. Jiang, W. Li, Z. Wen, Y. Bie, H. Schwarz, and C. Zhang, "Series arc fault detection based on random forest and deep neural network," *IEEE Sensors J.*, vol. 21, no. 15, pp. 17171–17179, Aug. 2021.
[21] S. Zhang, N. Qu, T. Zheng, and C. Hu, "Series arc fault detection based on wavelet compression reconstruction data enhancement and deep residual network," *IEEE Trans. Instrum. Meas.*, vol. 71, pp. 1–9, 2022.
[22] R. Chu, P. Schweitzer, and R. Zhang, "Series AC arc fault detection method based on high-frequency coupling sensor and convolution neural network," *Sensors*, vol. 20, no. 17, p. 4910, Aug. 2020.
[23] K. C. Paul, T. Zhao, C. Chen, Y. Ban, and Y. Wang, "Efficient-ArcNet: Series AC arc fault detection using lightweight convolutional neural network," in *Proc. IEEE Energy Convers. Congr. Expo. (ECCE)*, Vancouver, BC, Canada, Oct. 2021, pp. 1327–1333.
[24] Y. Wang, L. Hou, K. C. Paul, Y. Ban, C. Chen, and T. Zhao, "ArcNet: Series AC arc fault detection based on raw current and convolutional neural network," *IEEE Trans. Ind. Informat.*, vol. 18, no. 1, pp. 77–86, Jan. 2022.
[25] *General Requirements for Arc Fault Detection Devices*, Standard IEC62606, International Electrotechnical Commission, Geneva, Switzerland, 2017.

AIXIA TANG received the B.S. degree in electrical engineering from Yanshan University, Qinhuangdao, China, in 2008, and the M.S. degree in electrical engineering from Liaoning Technical University, Huludao, China, in 2011, where she is currently pursuing the Ph.D. degree in mine mechanical and electrical engineering.

Her current research interests include electrical contact and electric arc.

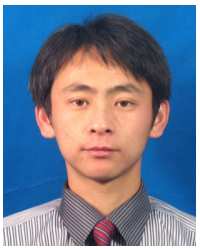

ZHIYONG WANG (Member, IEEE) received the B.S. and M.S. degrees in electrical engineering and the Ph.D. degree in safety management engineering from Liaoning Technical University, Huludao, China, in 2005, 2008, and 2017, respectively.

He is currently an Associate Professor with Liaoning Technical University. His current research interests include electrical contact, electric arc, and intelligent electrical apparatus.

SHIGANG TIAN (Student Member, IEEE) received the B.S. degree in electrical engineering from Liaoning Technical University, Huludao, China, in 2021, where he is currently pursuing the M.S. degree in electrical engineering.

His research interests include electric arc and intelligent electrical apparatus.

HONGXIN GAO (Member, IEEE) received the B.S., M.S., and Ph.D. degrees in electrical engineering from Liaoning Technical University, Huludao, China, in 2013, 2015, and 2019, respectively.

He is currently an Associate Professor with Liaoning Technical University. His current research interests include electrical contact, electric arc, and intelligent electrical apparatus.

YONG GAO received the B.S. degree in electrical engineering from Hubei Engineering University, Wuhan, China, in 2020. He is currently pursuing the M.S. degree in electrical engineering with Liaoning Technical University, Huludao, China.

His current research interests include electric arc and intelligent electrical apparatus.

FENGYI GUO (Senior Member, IEEE) received the B.S. and M.S. degrees in electrical engineering from the Fuxin Mining Institute, Fuxin, China, in 1987 and 1990, respectively, and the Ph.D. degree in electrical engineering from Xi'an Jiaotong University, Xi'an, China, in 1997.

He was a Visiting Professor with the University of Pretoria, Pretoria, South Africa, from 2002 to 2003, and Oxford University, Oxford, U.K., from 2008 to 2009. He is currently a Professor with Wenzhou University, Wenzhou, China. His current research interests include electrical contact, electric arc, and intelligent electrical apparatus.